Tribological properties of topographically structured polymer films

Master Thesis

Author(s):
Dusseiller, Marc R.

Publication date:
2001

Permanent link:
https://doi.org/10.3929/ethz-a-005321644

DIPLOMA THESIS WS00/01

LABORATORY FOR SURFACE SCIENCE AND TECHNOLOGY
DEPARTMENT OF MATERIALS, ETH ZÜRICH

TRIBOLOGICAL PROPERTIES OF TOPOGRAPHICALLY STRUCTURED POLYMER FILMS

Abstract

It was the goal of this study to reproduce results, obtained in the SFA, for a topographically structured polymer surface sliding on a flat counterface, using a state-of-the-art tribometer, modified to measure on a toroidal geometry. In addition, different regimes of loads and speeds were investigated, to determine the dynamics of the sliding system. Wear turned out to be a major problem, when structured polymers are slid against each other, and thus not all results were conclusive. No drastic reduction in friction force could be measured with structured surfaces. However, it could be shown, that some regimes of interest in tribology, which exist between the two techniques-the SFA and the tribometer-still lack fundamental understanding and an appropriate experimental technique. In addition, different ways to chemically and mechanically structure a polymer were investigated. A new and promising procedure has been developed for the controlled dewetting of polymers from topographical template structures.

Author:

Marc R. Dusseiller
Student, Department of Materials, ETH Zürich

Supervisors:
Dr. Manfred Heuberger, Dr. Kirill Feldman

...

In motorcycle maintenance the *mu* answer given by the machine to many diagnostic questions put to it is a major cause of gumption loss. It *shouldn't* be! When your answer to a test is indeterminate it means one of two things: that your test procedures aren't doing what you think they are or that your understanding of the context of the question needs to be enlarged. Check your tests and restudy the question. Don't throw away those *mu* answers! They're every bit as vital as the yes or no answers. They're *more* vital. They're the ones you *grow* on!

Zen and The Art of Motorcycle Maintenance
by Robert M. Pirsig

1 Introduction

1.1 General

In many applications regular surface structures, topographical or chemical, have revealed new effects and possibilities.[1] And also nature provides us with biological systems, optimized through evolution, which show excellent performance due to their surface structures (Fig 1.1). A shark, for example, reduces its drag, when it moves through water, by regularly ordered ribs on its skin.[1] Or the „lotus effect“, observed since early in history, which provides the lotus leaf with a water repellent and self cleaning surface. This is achieved by regular surface roughness and chemical structure.[1] As a last example the exceptional tribological properties of the attachment pads of insects is mentioned, which let them walk upside down on smooth surfaces like glass. This also is achieved by the surface microstructure in combination with biophysical adhesion phenomena.[2]

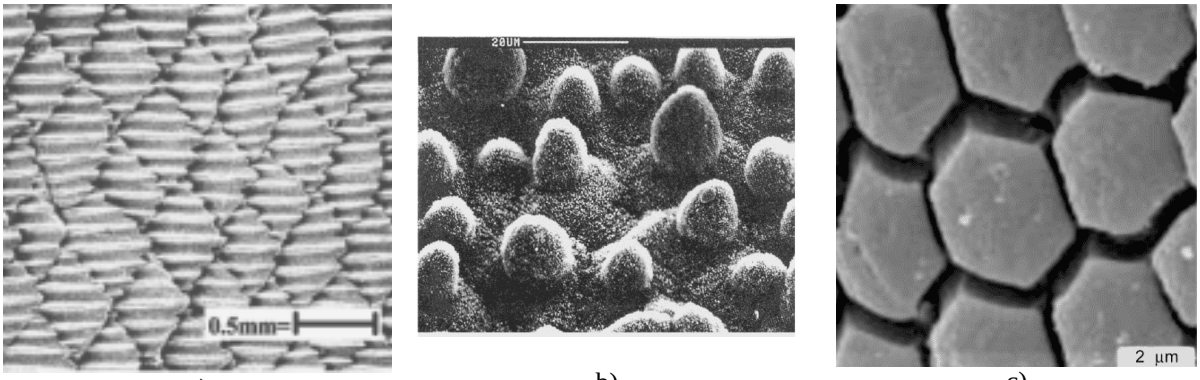

a) b) c)

Fig 1.1 Surface structures of different biological systems; a) shark skin;[1] b) surface of a lotus leaf;[1] c) insect attachment pad[2]

The tribological properties of patterned surfaces is also the focus of this study. Only little has been done so far in this field, but it seems to be very promising.

The possibility of reducing or tailoring the frictional properties by a simple structuring of the sliding surface might lead to many potential applications to reduce energy losses due to friction in small high-precision devices, such as micro electro-mechanical systems (MEMS), storage devices, gyroscopes or aerospace actuators.

1.2 Background

Earlier studies, using a surface forces apparatus (SFA) modified for measuring frictional forces, showed that the interfacial dynamics of the friction process can be modified (see below for further details) and states of vanishingly small friction can be reached by inducing

normal (out-of-plane) vibrations between two boundary-lubricated, flat sliding surfaces (Fig 1.2).[3]

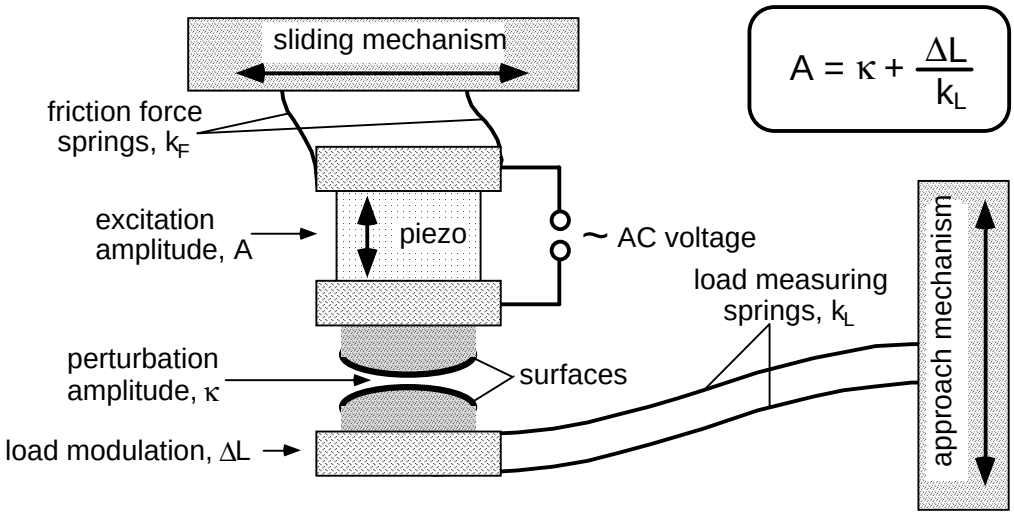

Fig 1.2 Schematic representation of the SFA experiment for the simultaneous measurement of normal load, L, and lateral friction force, F, with a piezo transducer to introduce oscillations into the sliding system; frequency range, f = 0 – 10 kHz; static load, L = 0 – 20 mN; sliding speed, v = 0 – 1 μm/s

These vibrations were coupled into the system by a piezo transducer. The amplitudes of these perturbations were below 0.1 nm and thus the influence on the normal force is negligible (<μN), because the spring constant of the load cell was k_L = 550 N/m. The results are shown in Fig 1.3.

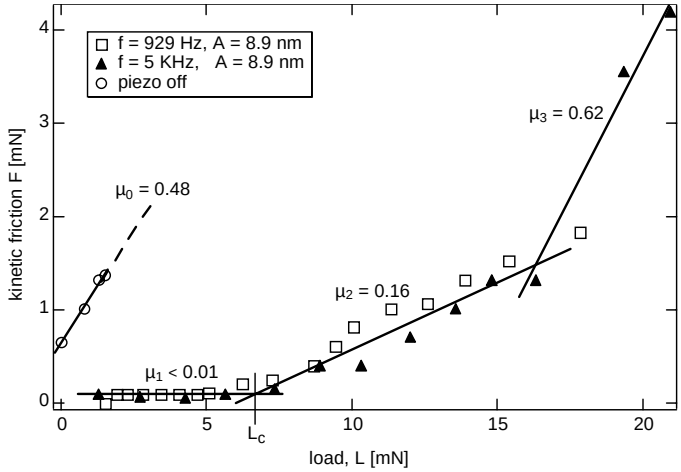

Fig 1.3 Kinetic friction force, F, measured as a function of the applied load, L, in three different dynamic situations (frequency, f = 0, 930, 5000 Hz). Driving piezo amplitude of excitation, 8.9 nm, sliding velocity, 58 nm/s. In the first regime near-zero kinetic friction is observed and the friction coefficient μ_1 was below the detection limit

Problems in these experiments were that the coupling of the normal force is always dependant on the resonance frequencies of the apparatus itself and can only be reached above a “main” resonance.[3] And although these experiments show practical conditions for producing low

friction, normal excitations are not easily applicable in a true sliding system. On the one hand simply because of the complexity of introducing an additional mechanism to produce these vibrations, the piezo transducer, into any application with desired low friction. On the other hand, the perturbations at the interface are also dependent on damping effects of the apparatus itself and not only on the external excitations.

These results gave rise to a new approach to coupling excitations into a sliding system; to topographically structure one surface of the sliding system. This leads to velocity dependent excitations at the interface, because one spot in the contact area is periodically in and out of contact with the counterface, due to the structured surface topography of the slider. The structure was a melt-embossed polymer film, FEP, which was slid against a flat counterface of the same material. First results obtained from SFA studies showed a reduction in friction force of 60 to 70 % (Fig 1.4) compared to sliding two unstructured surfaces. The exact mechanism leading to this reduction of friction has not yet been investigated. We believe that it is due to an effect similar to the mechanical excitations introduced by a piezo.

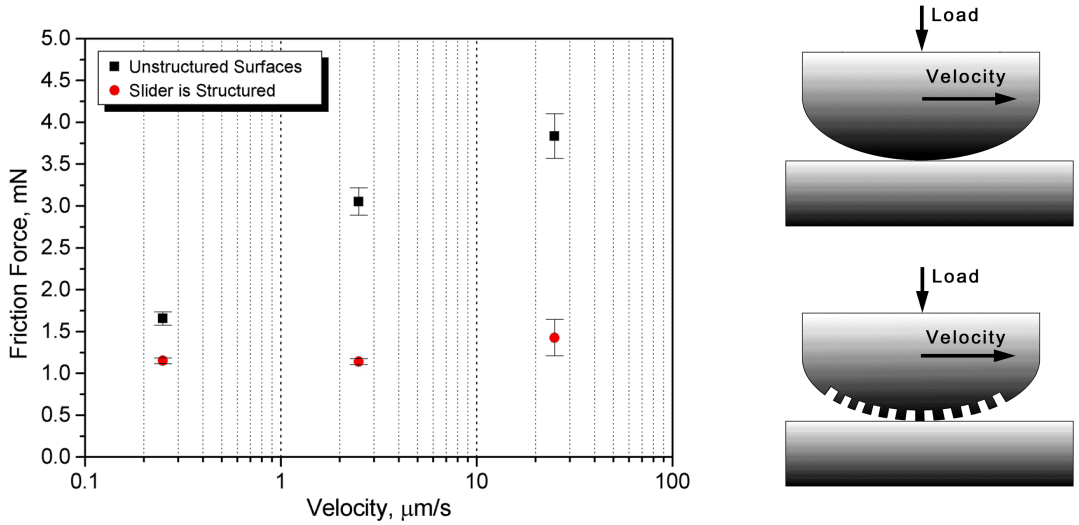

Fig 1.4 Results from friction measurements of flat and topographically structured PFA films performed in SFA; inset shows schematic model of experiment.

Another interesting approach to introduce an external excitation would be to use a mechanically/chemically structured surface instead of a topographical structured one (Fig 1.5). This could be realized on a flat surface, which eliminates any edge effects of the structure itself. Edge effects might lead to an increase in wear or other undesirable side effects. In a mechanically structured sliding system, for example, the interface sees a periodic change in elasticity of one surface, which is expected to produce similar effects as measured above.

(The theoretical background behind all these experiments is described below.)

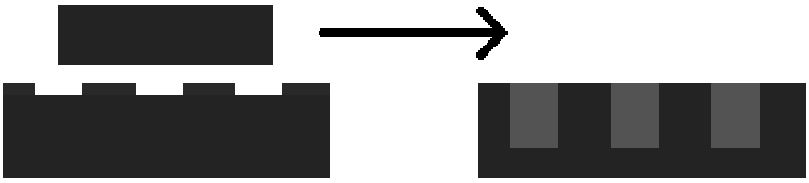

Fig 1.5 Topographical vs. chemical/mechanical structuring

1.3 Aim of this Study

The SFA is a technique for the study of fundamental phenomena in a well-defined system, although it can be difficult to translate any results into a true macroscopic tribological system. It is the aim of this study to reproduce the results mentioned above on a state-of-the-art tribometer. An overlap of different regimes in applied load and sliding speed is sought between SFA and tribometer. To use the same samples for both techniques, a toroidal disk was used in the tribometer to approximate the crossed cylinders of the SFA.

The frictional behavior of structured surfaces of the different polymers, FEP, PFA and UHMWPE, has been investigated.

In addition, the feasibility of simple ways to chemically/mechanically structure a polymer surface were investigated, trying different approaches.

2 Theory

2.1 Basics of Friction

Friction enables us to pick up a glass of water or drive a car. We have an intuitive understanding of friction. However, it is very difficult to formulate laws to fully describe the friction phenomenon.

Amontons' Law (2.1) provides us with a simple relation of applied load, L, and friction force, F, through the friction coefficient, μ. We note that the friction force is not dependent on the contact area, A, or the sliding speed, v. It serves well for most of the everyday uses of frictional behavior, but lacks the ability to describe the more fundamental processes in a frictional experiment.

Amontons' Law $F = \mu \cdot L$ (2.1)

Newer theories describe friction as the interaction of surface asperities sliding past each other and they also include a true contact area of these asperities instead of the macroscopic contact area. Friction is composed of the deformation, plastic or elastic, of these asperities. In many cases the true contact area is proportional to the load and thus it results in Amontons' law again.

The commonly used Bowden-Tabor equation (2.2) includes an additional term, which is dependent on the contact area, that takes adhesion effects into account, which show a big influence at low loads.[4]

Bowden-Tabor $F = \alpha \cdot A + \mu \cdot L$ (2.2)

2.2 Friction as a Dynamic Energy Dissipation Process

One way to view friction is by considering molecular dynamic relaxation processes at the sliding interface.[5] These become significant, when they are comparable to the timescale of observation, given by the sliding velocity, in a friction experiment. This approach is very suitable to describe the friction behavior of polymers and boundary lubricated systems.

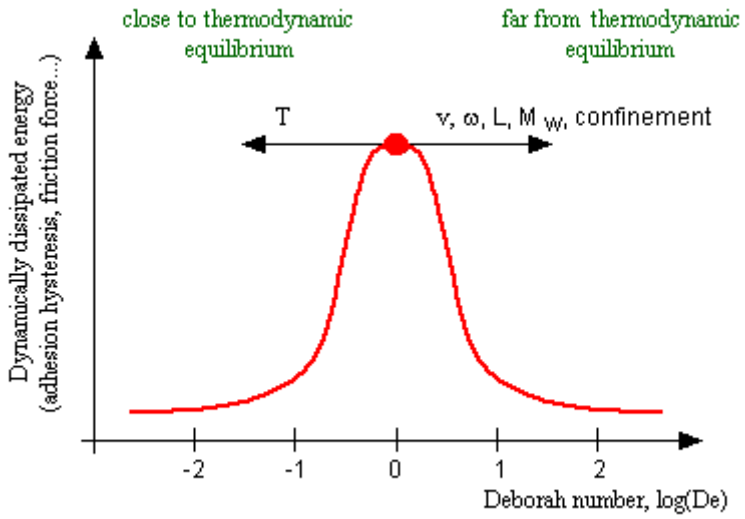

Fig 2.1 The *Deborah* number

The concept of the dimensionless *Deborah number*, De, which has its origins in the field of rheology,[6] has become common to describe the energy dissipation in kinetic friction experiments (Fig 2.1). In a simple form, the *Deborah number* equals the time of relaxation divided by the time of observation.

$$\textit{Deborah number} \qquad De_i = \frac{\tau_i}{\tau_{ext}} = \frac{\omega_{ext}}{\omega_i} = \frac{v_i}{v_{ext}} \tag{2.3}$$

Many polymers show a strong dependence of sliding velocity on friction, because relaxation processes are present in the material, which are on a similar time scale as some experiments. This results from a logarithm of the *Deborah number* around zero and a maximum of dissipated energy.[7-9]

The sliding speed can be increased by several orders of magnitudes and regime of superkinetic" friction can be achieved, as long as no other high frequency relaxation processes are present.[10] Also the influence of temperature, load and confinement (in boundary layers) can be explained using the *Deborah number*.

Another approach is, to introduce additional high frequency excitations into the sliding system to bring the system to a dynamic regime with low friction without changing the sliding speed.

3 Experimental

3.1 Materials

FEP and PFA (purum, Aldrich) in the form of beads; UMHWPE (Stamylan 210, $2*10^6$ M_w) was cast as film from a 2 wt% solution in m-xylene; HDPE beads (Stamylan 6480); iPP beads (Montell); Fluorinert™ Fluid FC-77 (Fluka) was used as lubricant; the high-precision cylinders were made of SiO-glass; the silicon gratings, TGZ02, TGZ03, TGG01, TGX01, used as shims are AFM calibration gratings by NT-MDT (see Appendix I), which were fluorinated to avoid sticking; fluorinated silicon wafers were used as flat shims; different wt% solutions of PS in m-xylene (purum, Fluka) and toluene (purum, Fluka); the mold was machined from steel.

3.2 Toroidal Tribometer Geometry

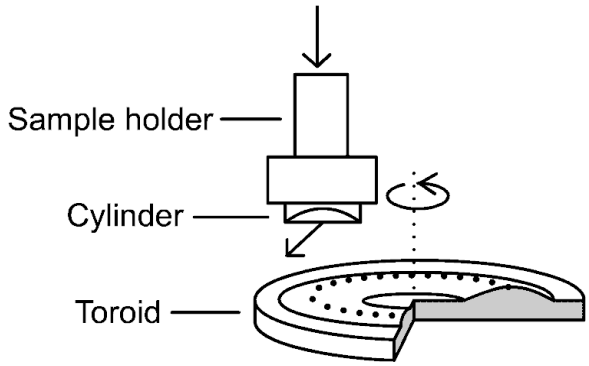

Fig 3.1 The troidal geometry

The toroidal geometry (Fig 3.1) is very similar to the commonly used ball-on-disc tribometer, in fact the contact geometry of two crossed cylinders is equivalent to a ball-on-flat surface. Surface treatments, e.g. structuring, on rounded surfaces, as balls, very often raise insoluble problems. This system allows the user to apply any surface treatment on a flat film, which is then bent and attached onto the cylinder. The curvature radius of the toroid / cylinder was 15 mm and 20 mm respectively. The whole system was used in an ordinary tribometer, as described below.

3.3 Sample Preparation

3.3.1 Toroidal Disks

The first toroidal disks were produced in a press-mold process involving a steel tube, a brass cylindrical piston and a steel mold. However, problems occurred with temperature control and

equilibrium, due to the large thermal mass of the mold, and the polymer partially degraded after the 1h-long process. Additionally, demolding of the disk was very difficult, because of strong adhesion of the polymer to the mold. Thus, a new flat design was developed as seen in Fig 3.2, see Appendix II for further details. It showed better temperature control at the disk itself and thus processing time could be reduced. Also, demolding was easier because the toroidal inset could be screwed out, creating enough shear force to break the interface polymer/mold.

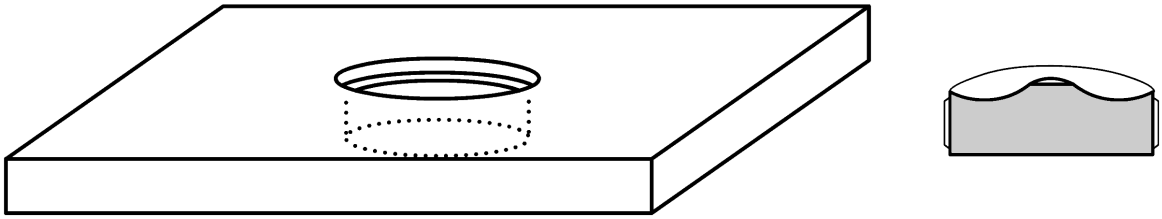

Fig 3.2 New mold design; plate with a screwed hole and toroidal inset with screw

The mold was filled with polymer beads, the weight was calculated from the volume of the toroid, with an excess of 10 to 20%. It was covered with an aluminum sheet and put into a hot press at elevated temperature. Before pressing, the mold was thermally equilibrated for 10 min. Then it was pressed for another 5 minutes with a pressure of 4 t. Afterwards, the mold was directly quenched in a second water cooled press at low pressure. The processing temperatures for the different polymers are as follows; FEP at 330°C, PFA at 350°C, HDPE at 180°C.

Between every process the negative toroidal inset was polished with a fine paste and subsequently cleaned.

For the UHMWPE toroid, a film of UHMWPE (thickness ~ 200 μm) was welded onto a HDPE-toroid by pressing it together in the mold at 180°C and subsequently quenched again.

The curvature of one UHMWPE toroid was measured with the CETR tribometer, using a sharp steel pin which was moved from the center outwards (Appendix II).

3.3.2 Structuring the Films

Films of FEP and PFA were pressed using a Tribotrak press (DACA Instruments). A single bead was pressed between two glass slides, with increasing loads, 100 g, 200 g, 500 g, 1000 g, each load being exerted for 1 min. The solution-cast UWMWPE-films were recrystallisated in a hot press for 10 min with a load of 4 t.

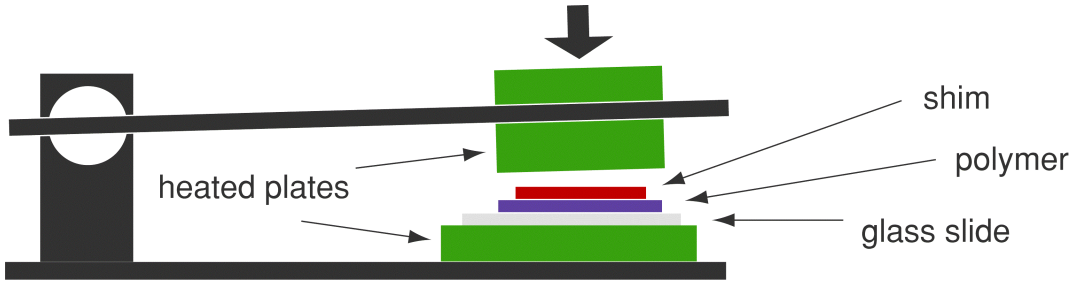

Fig 3.3 Melt embossing on a Tribotrak press

The structures were melt-embossed[11,12] as seen in Fig 3.3, the processing parameters are listed in Table 1. To produce flat samples a square (4x4 mm) piece of Si-wafer was used, instead of the grating.

Table 1 Processing parameters of melt-embossing

Material	temperature	weight	time
FEP	330 °C	200 g	20 s
PFA	350 °C	200 g	20 s
UHMWPE	180 °C	2500 g	10 s

A 3x3 mm embossed area of the samples was cut out and plasma treated (Harrick PDC-32G) for 2 minutes to improve adhesion. Finally it was glued on the glass cylinder in the desired direction, either perpendicular or parallel to the sliding direction. The PFA samples were glued on with epoxy resin on a hot-stage at 113 °C, the UHMWPE samples with Patex Sekundenkleber Slalom.

3.4 Tribology

The first measurements of FEP and PFA were performed on a CSEM Pin-on-Disk tribometer with modified sample holders to attach the cylinder and the toroid. The load applied was 0.5 N. The measuring speed ranged from 0.1 to 25 RPM, approximately 0.1 to 25 mm/s.

Later, measurements of UHMWPE and PFA were performed on the CETR instrument (UMT-2 Multi Specimen Test System, see Appendix III) with Fluorinert™ FC-77 as lubricant. The CETR works with a load cell with a spring constant of 5 N/m, leading to a resolution of 3 * 10^{-3} N. The system works with a load feedback loop; friction force, load, spindle position and sample height were recorded. Applied load was 0.1 N for most measurements, unless stated otherwise. The first measurements were done over several revolutions. Later, only over a distance of 0.1 revolution, 6 mm, and then returned to the starting point. Speed range was measured from 0.025 to 0.8 RPM, 25 to 800 μm/s.

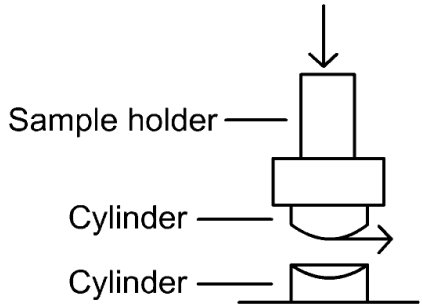

Fig 3.4 Linear friction measurements

Finally, measurements of UHMWPE were performed with CETR, modified for linear friction measurements, of one cylinder sliding over another in a rectangular position (Fig 3.4), sliding distance 5 mm, speed from 21 to 833 μm/s. These measurements were performed unlubricated and lubricated.

3.5 Chemical/Mechanical Structuring

3.5.1 Approaches

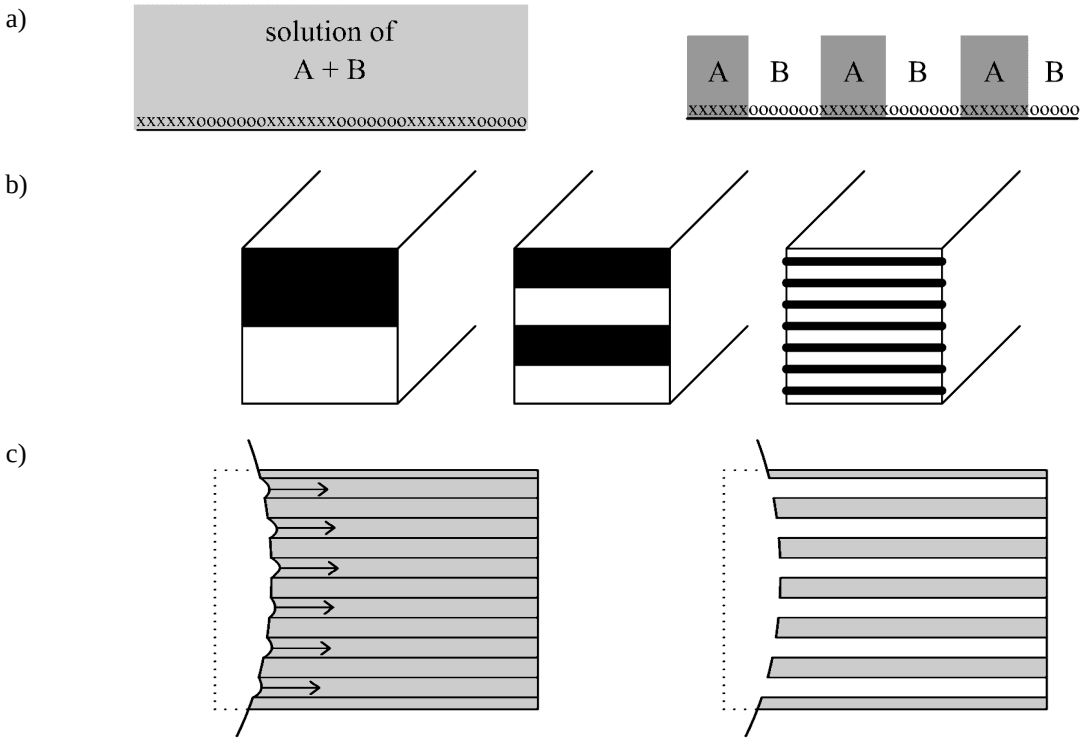

Fig 3.5 Different approaches to produce a chemically/mechanically structured surface;
a) Steiner method[13-15], b) static mixing, c) MIMIC[16,17]

Three different approaches were investigated (Fig 3.5). a) The Steiner method[13-15], to cast a film from a solution of two inmiscable polymers onto a gold coated substrate, which is structured chemically by micro contact printing[15]; b) static mixing of two different polymers

and subsequent cutting perpendicular to the plane of the layers; c) micromolding in capillaries (MIMIC)[16,17] to fill the grooves of a melt-embossed film.

3.5.2 Experiments

For the Steiner method a solution of PS and PEO (1 wt% each) in benzene was prepared. Gold-coated Si-wafers were used as a μ-cp substrate, which were structured with CH_3-terminated thiols using a PDMS stamp (TGZ structure like the Si-gratings) and afterwards dipped into a solution of OH-terminated thiols to attach to the unstructured gold surface. To apply a thick film of polymer on it, a drop of the solution was put onto the structured area, which was then covered and left until the solvent evaporated.

Samples, extruded by a static mixer, of PE mixed with PS were received from TU Eindhoven, thickness ~1 mm. It was the goal to hot-press a stack of several samples to increase the thickness. Unfortunately, the samples delaminated very easily when handling them, because of lack of adhesion between the layers, and this route was not continued further.

In first attempts of MIMIC, a drop of a 2 wt% PS solution in toluene, later in m-xylene, was placed on the edge of the structured area of a melt-embossed PFA film (TGZ03 and TGZ02) or iPP in some cases. Another attempt was to put a melt-embossed film upside down on a silicon wafer, to cover the grooves and thus create real capillaries, and placing a drop of solution on the edge of the sample.

Finally, structured PFA films were dip coated in a solution of PS, 2 and 20 wt% in m-xylene, and drawn at different speeds, which was achieved by lowering a lab table by hand. The same was also done with samples treated in plasma for two minutes.

3.5.3 Analysis

The samples were analyzed with an optical microscope. Some selected samples were further analyzed with atomic force microscopy (AFM).

4 Results and Discussion

4.1 Sample Preparation

4.1.1 Toroidal Disks

Almost all toroids pressed from beads showed some air bubbles inside the bulk (Fig 4.1), because the air could only flow out close to the upper edge of the mold. This problem can be eliminated by hot-pressing a dense cylindrical preform with a diameter of 15 mm into the mold. But the attempts to press cylindrical preforms also let to porous bodies most of the time, and did thus not improve the final toroid. But because in most samples the bubbles were well below the curved surface, it was not a problem to continue with them.

Fig 4.1 PFA toroid with some bubbles, diameter 30 mm

4.1.2 Structuring the Films

The melt-embossing technique showed a good reproduction of the topography of the gratings into all polymers used, as was observed under optical microscope.

4.2 Tribology

4.2.1 FEP and PFA on CSEM Tribometer

There was far too much wear during the experiment. The structures were completely worn away after measuring over several revolutions. FEP in particular, showed very bad properties. Because the load cannot be reduced on the CSEM instrument, due to noise and to the resolution of the machine, further experiments were thus performed on CETR.

4.2.2 PFA on CETR Tribometer

When the first measurements with 0.1 N load still showed problems with wear, the sliding distance was reduced and measurements were performed under lubricated conditions. However, the PFA samples still showed too much wear, even during a single measurement. The results could therefore not be reproduced. Fig 4.2 shows a reduction in friction after several experiments due to wear, which is described below.

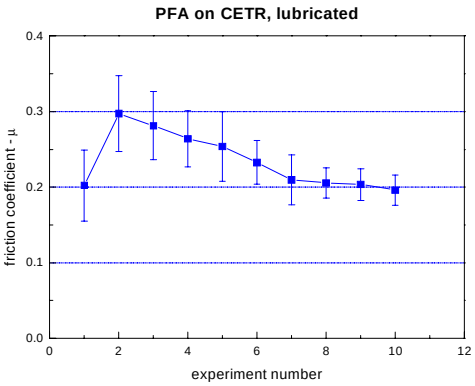

a)

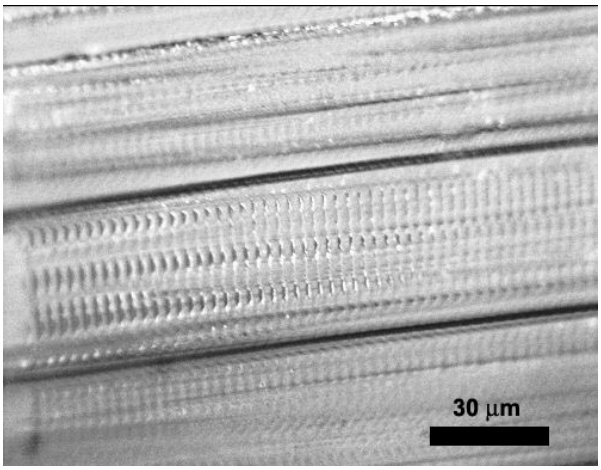

b)

Fig 4.2 a) First set of measurements show reduction of friction due to wear, load 0.1 N, speed 0.1 RPM; b) worn surface structure of PFA

4.2.3 UHMWPE on CETR Tribometer

Better results could be obtained when UHMWPE, known as a low wear material, was measured.[18] There was still a certain amount of wear, especially in the first couple of measurements. In Fig 4.3 one can see how the friction force decreases to a more stable value after several measurements. During these first measurements a lot of wear was observed, when the samples were checked under microscope. The wear trace showed a number of scratches through the structures (see Appendix IV for detailed pictures). These scratches derive from asperities, present on the toroid, which plough through the surface. After this ploughing, the load is distributed more evenly on other asperities in the contact area and plastic deformation of the structure is reduced. This also explains the reduction in friction after several experiments.

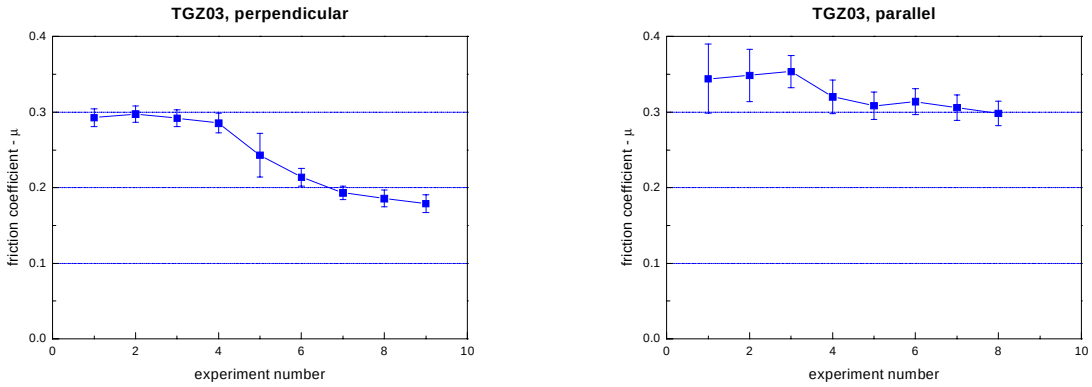

a) b)

Fig 4.3 First set of measurements show reduction of friction coefficient due to wear; UHMWPE, load 0.1 N, speed 0.1 RPM; a) TGZ03 perpendicular to the direction of sliding; b) parallel to the direction of sliding

Because of this it was very important that the position of the sample was not changed during the experiments, so that no new grooves could be ploughed, upon increasing the friction force. Taking this into account, most results were not very conclusive and great care had to be taken when different measurements were compared.

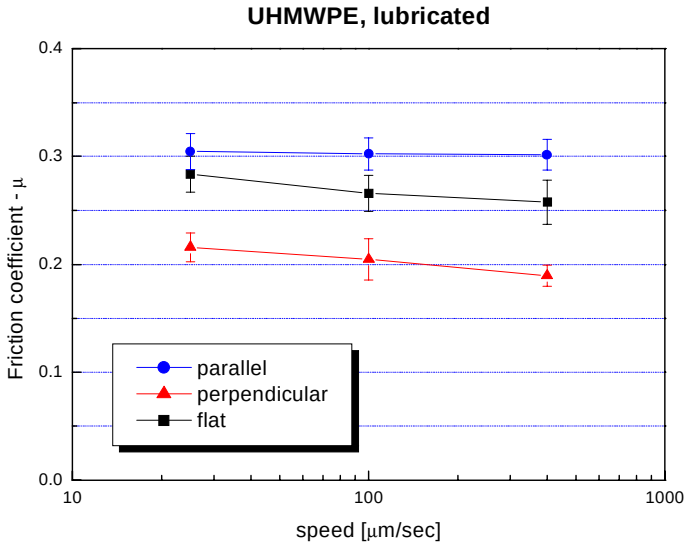

Fig 4.4 Friction coefficient of UHMWPE under lubricating condition at different speeds, measured on toroidal geometry, 0.1 N load; flat compared to TGZ03 structure perpendicular and parallel to the direction of sliding

In Fig 4.4 the most reproducible results are shown, comparing a flat sample to a TGZ03 structure, which was oriented either perpendicular or parallel to the direction of sliding. In these experiments a reduction in friction of roughly 25 % could be observed with the perpendicular structure.

The same reduction of friction force was also observed when measured at lower loads (Appendix V), but due to the resolution of the CETR it was difficult to obtain exact results.
The results obtained from other structures, TGG and TGX, can be found in Appendix V. They showed much wear and great care has to be taken when comparing with the results shown here.

4.2.4 UHMWPE on Linear CETR Tribometer

To reduce this ploughing effect of single asperities and the running in of the samples, the roughness of the counterface had to be reduced. This, was not possible with the toroid because of the roughness present on the negative mold, and thus the tribometer was modified to measure linearly over another cylinder. A flat film, which was pressed under a Si-wafer, could be glued onto the cylinder.
The running in effect could be essentially eliminated. Although wear was not reduced, it was more evenly distributed on the whole contact area (Appendix IV).

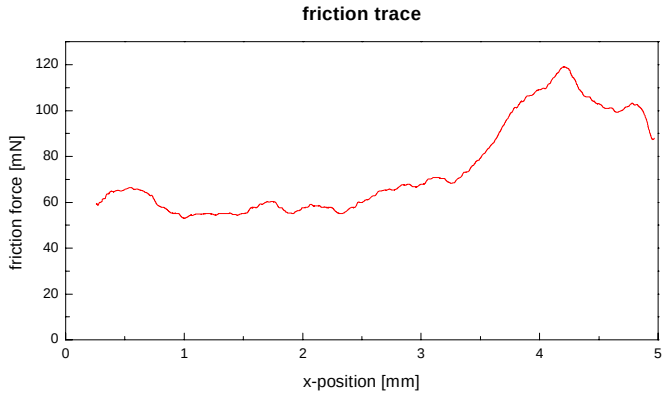

Fig 4.5 Friction trace of one single measurement over 5 mm of UHMWPE, flat on flat, load 0.1 N, speed 0.1 RPM

As long as the relative position of the cylinders was not changed the results were very reproducible. Upon changing relative position, the friction values changed by around 20 %. Also, the friction values during one single measurement scattered a lot more then earlier measurements (Fig 4.5). Thus a large error bar has to be included in all the results achieved by these experiments.
The results, shown in Fig 4.6, show a slight increase in friction force when the structured surfaces are compared to a flat sample, but due to the large error bar, great care has to be taken to draw this conclusion.
When these measurements were finally performed under lubricated conditions, no reproducibility was observed at all. While some results resembled the shape of the

unlubricated measurements, shown in Fig 4.5, others showed a flat and stable value around 20 mN, without changing anything in the experiment, see Appendix V. Possible explanations are given below.

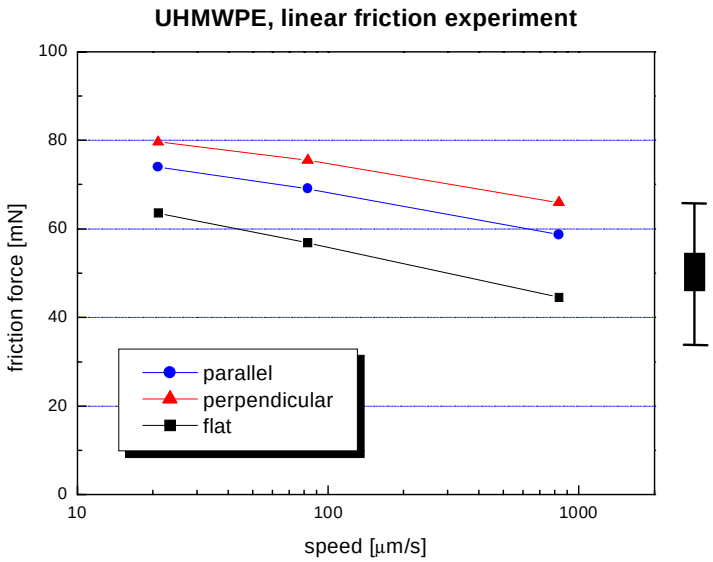

Fig 4.6 Friction force of UHMWPE at different speeds measured on linear tribometer, no lubrication, 0.1 N load; flat compared to TGZ03 structure perpendicular and parallel to the direction of sliding

4.2.5 Regimes of Tribology

The step from the well-defined SFA experiments to a common tribometer turned out to be more difficult than expected. Fig 4.7 shows the regimes that can be covered by the different techniques[19] and the regimes of interest in this work.

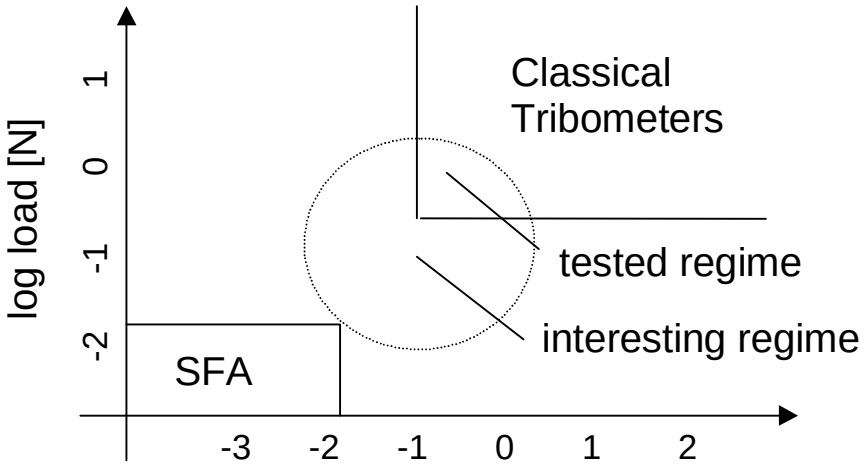

Fig 4.7 Regimes of tribology

In the SFA, one single and well-defined asperity contact is measured and only small loads and speeds can be applied, while the classical tribometers are used at higher loads and speeds. Thus, in a tribometer, a statistically very large number of asperity contacts are present in the apparent contact area. This leads to an averaging of the total friction force that is measured over all the contact points. When the load is decreased, however, the number of contacts decreases as well. Below a certain limit, the statistical averaging is less efficient and it becomes more difficult to measure exact and reproducible friction forces. This gets even more crucial when the roughness is decreased at these low loads, as in the experiments above. By doing so, the geometry and distribution of the asperity contacts changes and the system is much more dependant on small differences present on the surface (Fig 4.8).

Fig 4.8 Model of contact area, different asperity contact geometry and distribution; a) rough; b) smooth surface

Under lubricated conditions, the systems become even more complex,[20,21] because most areas in the apparent contact area are in a mixed lubrication regime, while the asperity contacts are under boundary lubrication conditions. This leads to very variable conditions in the experiments.

The experiments described above, of course, cannot provide a fundamental understanding of the important processes present under these circumstances, but gave rise to the ideas described here.

4.3 Chemical/Mechanical Structuring

4.3.1 Steiner Method

While Steiner achieved structured thin films (~ 100 nm) by spin coating, it turned out to be difficult to produce a thicker film which can be handled to use for friction measurements. When the solvent evaporated from the drop of solution, one could observe that crystallization was induced from the liquid/air surface rather than from the structured gold surface. Even when covered, in order to saturate the surrounding air and reduce the speed of evaporation, the samples did not satisfy our requirements.

One way to solve the problem would be to spin coat on the structured gold surface, thus producing a thin film, onto which another thick layer of polymer is subsequently welded. The thick film then has to be removed from the gold substrate and a flat and structured surface is produced. Because of the small depth of the structured material, these film can only be used for friction measurements involving low wear, but they might be very interesting to analyze in the SFA.

4.3.2 First Attempts in MIMIC

Because toluene was too volatile, it was difficult to perform the MIMIC experiments and thus m-xylene was further used as solvent for PS. Initial experiments performed with a 2 wt% solution of PS in m-xylene on TGZ structured PFA showed no rise of the liquid in the capillaries. The capillary force was pointing in the wrong direction, because the solution did not wet the PFA surface.[16] Thus iPP was used instead, since it is wettable. However, the advance of the liquid only reached a few μm (Fig 4.9). The capillary forces were still too small to drag the liquid through the whole structure before the solvent evaporated, because no true capillaries are present on the structure, only three sided grooves.

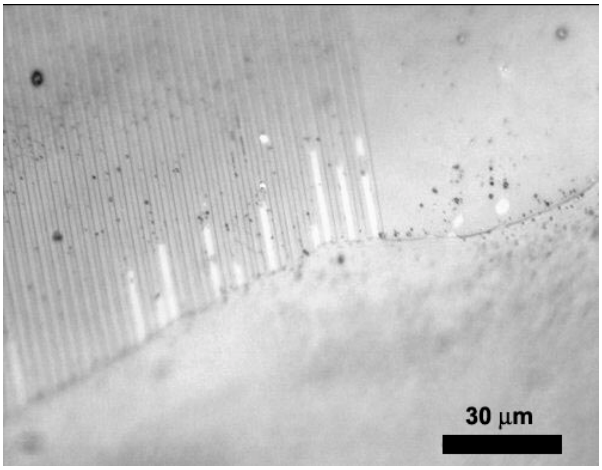

Fig 4.9 Capillary advance of PS solution on TGZ03 structured iPP (MIMIC)

The experiments performed with the structure upside down on a Si-wafer, to account for the fourth side, were not successful either, because the liquid flowed underneath the sample and lifted it off.

4.3.3 Dip Coating

The dip coating experiments showed remarkable results. When withdrawn at slow speed, almost all lines of the structure could be filled with PS and no remaining PS could be found on top of the structure (Fig 4.10).

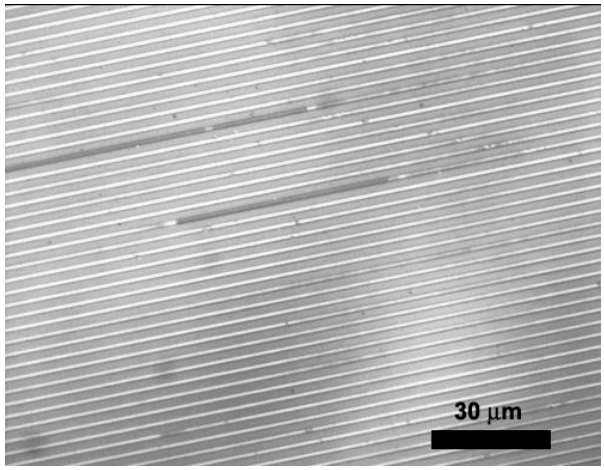

Fig 4.10 TGZ03 structured PFA, no plasma treatment, almost all lines filled with PS; bright lines are grooves containing PS

The topography of a cross-section is shown in Fig 4.11 a. It can be seen that one groove is completely empty and shows the same geometry as the untreated grooves, while in the two other grooves partial filling with PS was achieved. Even when dip coated in a 20 wt% solution, complete filling of the grooves was not achieved (Fig 4.11 b). The thickness of the PS layer in the groove, 2 % and 20% solution, was 80 nm and 150 nm respectively. More pictures can be found in Appendix VI.

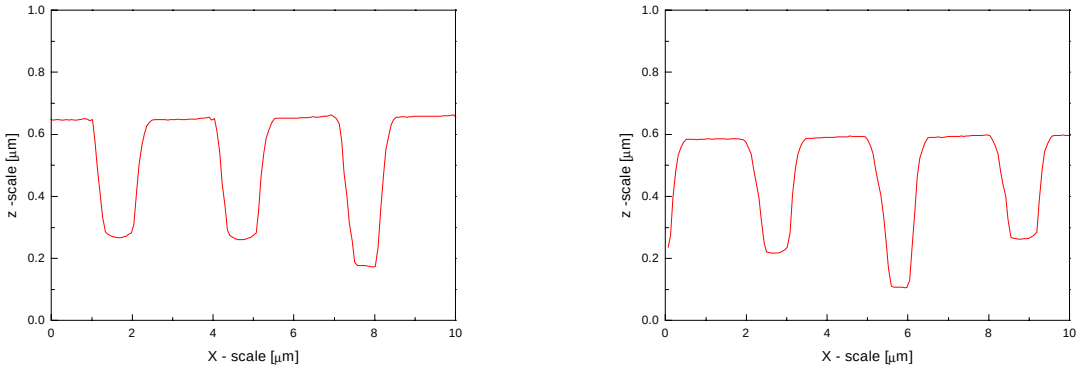

a) b)

Fig 4.11 AFM topography line scan perpendicular to the structure; a) dipped in 2 wt% solution; b) 20 wt%

When the PFA surface was plasma treated before dip coating, a film of PS could be deposited on top of the whole structure (Fig 4.12). No contrast could be observed when scanned in the lateral force mode in AFM. The PS solution apparently did not dewet from the PFA surface.

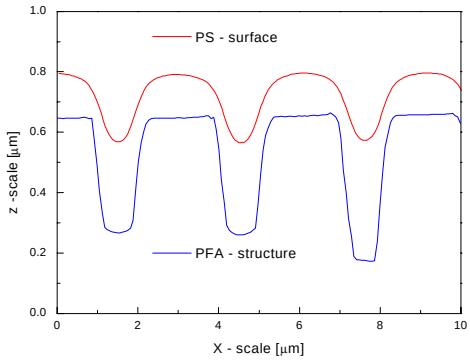

Fig 4.12 AFM topography line scan of a PS layer on top of a plasma treated surface topography; thickness of PS film estimated

4.3.4 Conclusion

The results obtained by dip coating can be explained as follows. The PFA surface, when not plasma treated, is not wettable by the solution. Under these circumstances, dip coating is not possible on a flat surface. This is different when a topographical structure is present. When the liquid retreats from the surface, it is trapped in the groove, where it forms a contact angle above 90 ° with the sides of the groove. A force is established, whose magnitude depends on the curvature of the liquid surface, pointing inwards the groove (Fig 4.13). Thus the liquid drop does not retreate once it is inside the groove. When the solvent evaporates, what remains is a thin layer of polymer at the bottom of the groove.

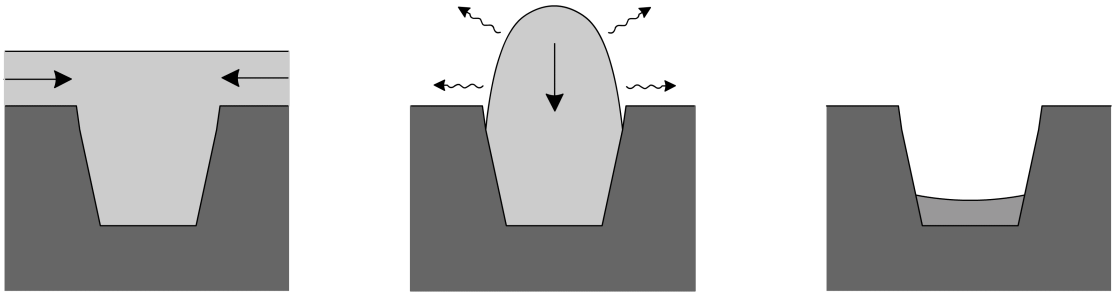

Fig 4.13 Model of dewetting top surface and wetting in the grooves and subsequent evaporation of the solvent

The thickness of this layer depends on the shape of the stable drop, formed after coating. Thus the grooves could not be filled much more when a higher concentration of PS in the solvent was used, because the surface energy of the liquid was changed and thus the geometry of the trapped liquid is also modified.

With an optimized selection of solvents, materials and withdrawal speed, it might be possible to completely fill the grooves.

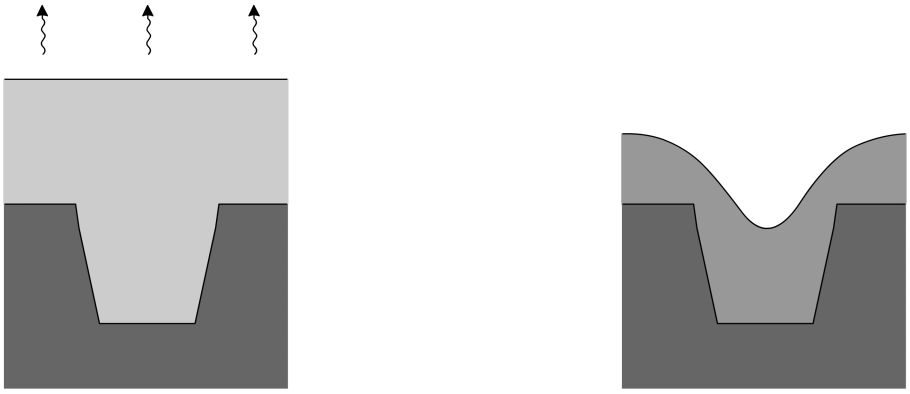

Fig 4.14 Model of dip coated plasma treated sample

When the surface is plasma treated, or in general made wettable by the liquid, the crucial dewetting step of the top structure to form the trapped drop is not present. What results is a coated topographical structure, which is smoothed out by the layer of polymer on top of it (Fig 4.14).

With this method more material can be deposited on the structure. It might still be possible, that this layer dewets from the top surface and retreats into the grooves when annealed at temperatures above the T_G of PS. This is because the influence of the plasma treatment is not permanent and PS might then dewet into the grooves.

5 Conclusion and Outlook

The toroidal geometry that has been developed, offers new possibilities in tribological experiments, when the classical ball-on-disk geometry is not suitable. Any surface treatment can be applied to flat films, which can be easily attached onto a cylinder, as long as the film is flexible enough. Toroidal disks can be produced from various materials with an appropriate processing technique; for example metals can be formed by machining, ceramics by slurry casting and polymers by press molding.

It has also been shown that the regime of interest between the SFA technique and most tribometers is still difficult to describe and to measure.[19] Thus, the application of the fundamental understanding of friction processes gained from SFA experiments to a larger scale tribological system is still problematic. To gain further knowledge of the friction processes in the unknown regime, an overlap of the two techniques has to be sought. In particular, the speed range of the SFA technique has to be expanded (Fig 5.1). This is most important when the dynamics of a sliding system is investigated, since dynamic processes always extend over several orders of magnitude. It is also important to gain further knowledge in these regimes, to describe friction processes in modern micro mechanical applications.

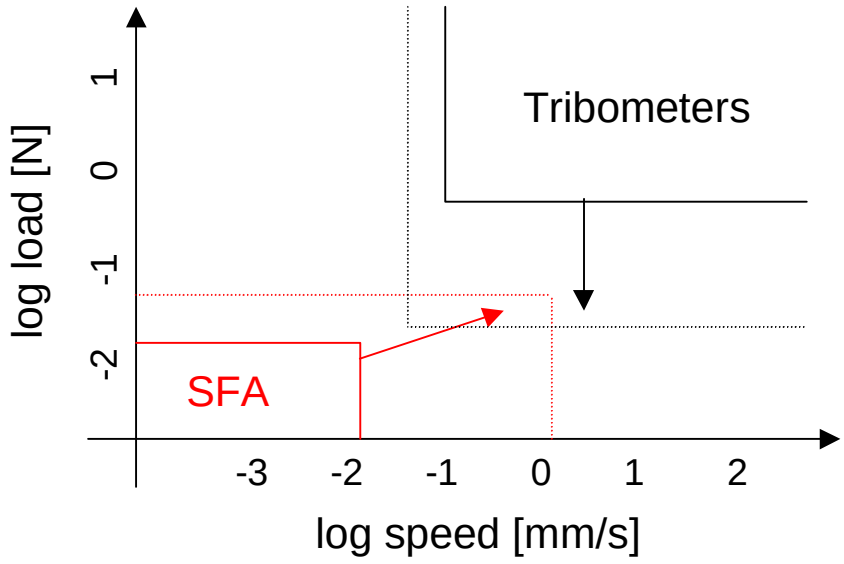

Fig 5.1 Overlap of different techniques by expansion of measurable loads and speeds

Due to the problems occurring during the experiments described above, it was not possible to measure the influence of the topographical structures on the dynamics of the friction process. A clear reduction, or change, in friction force of the structured surfaces could not be shown

under unlubricated conditions. In general, wear turned out to be a major problem in any application that includes topographical structures. Thus it might only be applied to systems with small loads and low wear conditions

Under lubricated conditions, however, a reduction in friction could be observed, when the structure was slid perpendicular to the direction of sliding. Although it is not yet clear wether this reduction is due to a change of the interface dynamics or, as has also been reported earlier[22], to a different lubricant supply in the contact area. This last aspect might also be very interesting in many lubricated systems, where lubrication can not be guaranteed over the whole contact area of a flat surface.

A new process has been found to use a topographical guiding template to produce spatially seperated polymer structures. This process shows many advantages over similar processes including μ-cp or photolitography, because of its simplicity and low production cost.[23-25]

Of course, this new process has to be investigated further, in order to find its limits in application on different length scales of the structures. The approach needs optimization in terms of withdrawal speeds, materials and concentrations. It should be possible that certain structures might be completely filled with another material with the right choice of parameters, resulting in a chemically/mechanically structured flat surface. Tribological experiments could be performed on samples of this kind using theSFA as mentioned in the introduction, which might show interesting results.

6 Acknowledgements

Dr. M. Heuberger, Dr. K. Feldman, Prof. N. D. Spencer,

Laboratory of Surface Science and Technology,

Department of Materials, ETH Zürich

Institute of Polymer Technology,

Department of Materials, ETH Zürich

Institute of Non-Metallic Inorganic Materials,

Department of Materials, ETH Zürich

7 References

(1) Bechert, D.W.; Bruse, M.; Hage, W.; Meyer, R. „Fluid Mechanics of Biological Surfaces and their Technological Application“, *Naturwissenschaften*, **2000**, 87, 157.

(2) Scherge, M; Gorb, S.N. „Microtribology of Biological Materials“, *Tribology Letters*, **2000**, 8, 1.

(3) Heuberger, M.; Drummond, C.; Israelachvili, J. „Coupling of Normal and Transverse Motions during Frictional Sliding“, *J. Phys. Chem. B*, **1998**, 102, 5038.

(4) Arnell, R.D.; Davies, P.B.; Halling, J.; Wholmes, T.L., *Tribology – Principles and Design Applications*, Macmillian Education LTD, London, 1991.

(5) Tabor, D. „Friction as a Dissipative Process“. In *Fundamentals of Friction: Macroscopic and Microscopic Processes*; Singer, I.L.; Pollock, H.M., Ed.; NATO ASI Series E: Applied Sciences; Kluwer Academic Publishers: Dordrecht, 1992, Vol. 220, p 3.

(6) Reiner, M „The Deborah Number“, *Physics Today*, **1964**, January, 62.

(7) Israelachvili, J.; Berman, A. „Irreversibility, Energy Dissipation, and Time Effects in Intermolecular and Surface Interactions“, *Israel Journal of Chemistry*, **1995**, Vol. 35, 85.

(8) Heuberger, M.; Luengo, G.; Israelachvili, J.N. „Tribology of Shearing Polymer Surfaces. 1. Mica Sliding on Polymer (PnBMA)“, *J. Phys. Chem. B*, **1999**, 103, 10127.

(9) Luengo, G.; Heuberger, M.; Israelachvili, J.N. „Tribology of Shearing Polymer Surfaces. 2. Polymer (PnBMA) Sliding on Mica“, *J. Phys. Chem. B*, **2000**, 104, 7944.

(10) Yamada, S.; Nakamura, G.; Amiya, T. „Shear properties for Thin Films of Star and Linear Polymer Melts“, *Langmuir*, **2001**, 17, 1693.

(11) Gale, M.T.; „Replication Technology for Holograms and Diffractive Optical Elements“, *Journal of Imaging Science and Technology*, **1997**, 41, 211.

(12) Stutzmann, N.; Tervoort, T.A.; Bastiaansen, C.W.M.; Feldman, K.; Smith, P. „Solid-State Replication of Relief Structures in Semicrystalline Polymers“, *Advanced Materials*, **2000**, 12, 557

(13) Böltau, M.; Walheim, S.; Mlynek, J.; Krausch, G.; Steiner, U. „Surface-Induced Structure Formation of Polymer Blends on Patterned Substrates“, *Nature*, **1998**, 391, 877.

(14) Böltau, M.; Walheim, S.; Mlynek, J.; Krausch, G.; Steiner, U. „Structure Formation via Polymer Demixing in Spin-Cast Films“, *Macromolecules*, **1997**, 30, 4995.

(15) Karim, A.; Douglas, J.F.; Lee, B.P.; Glotzer, S.C.; Rogers, J.A.; Jackman, R.J.; Amis, E.J.; Whitesides, G.M. „Phase Seperation of Ultrathin Polymer-Blend Films on Patterned Substrates“, *Physical Review E*, **1998**, 57, 6273.

(16) Kim, E.; Xia, Y.; Whitesides, G.M. „Polymer Microstructures Formed by Molding in Capillaries“, *Nature*, **1995**, 376, 581.

(17) Kim, E.; Xia, Y.; Whitesides, G.M. „Micromolding in Capillaries: Applications in Material Science“, *J. Am. Chem. Soc.*, **1996**, 118, 5722.

(18) Klapperich, C.; Komvopoulos, K.; Pruitt, L. „Tribological Properties and Microstructure Evolution of Ultra-High Molecular Weight Polyethylene“, *Journal of Tribology*, **1999**, 121, 394.

(19) Kaneko, R. „Some Recent Progress in Microtribology in Japan“, *Tribology Letters*, **2000**, 9, 89.

(20) Luengo, G.; Israelachvili, J.; Granick, S. „Generalized Effects in Confined Fluids: New Friction Map for Boundary Lubrication“, *Wear*, **1996**, 200, 328.

(21) Hu, Y.Z.; Wang, H.; Wang, W.Z.; Zhu, D. „A Computer Model of Mixed Lubrication in Point Contacts“, *Tribology International*, **2001**, 34, 65.

(22) Blatter, A.; Maillat, M.; Pimenov, S.M.; Shafeev, G.A.; Simakin, A.V., Loubin, E.N. „Lubricated Performance of Laser-Patterned Sapphire“, *Wear*, **1999**, 232, 226.

(23) Darhuber, A.A.; Troian, S.M.; Davis, J.M.; Miller, S.M. „Selective Dip-Coating of Chemically micropatterned Surfaces“, *J. Appl. Phys.*, **2000**, 88, 5119.

(24) Meyer, E.; Braun, H.-G. „Controlled Dewetting Processes on Microstructured Surfaces – a New Procedure for Thin Film Microstructuring“, *Macromol. Mater. Eng.*, **2000**, 276/177, 44.

(25) Vaeth, K.M.; Jackman, R.J.; Black, A.J.; Whitesides, G.M.; Jensen, K.F. „Use of Microcontact Printing for generating Selectively Grown Films of Poly(p-phenylene vinylene) and Parylenes Prepared by Chemical Vapor Deposition“, *Langmuir*, **2000**, 16, 8495

APPENDIX I

Silicon gratings manufactured by NT-MDT

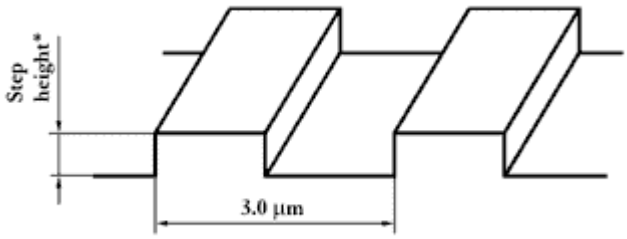

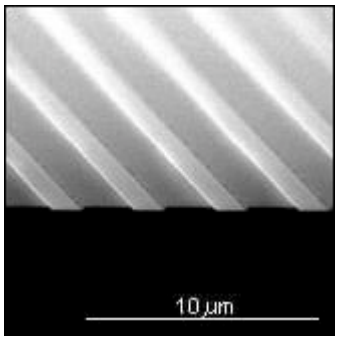

TGZ; Step height*02, 114 nm, *03, 512 nm, 3 lines of structured area of 1 * 3 mm

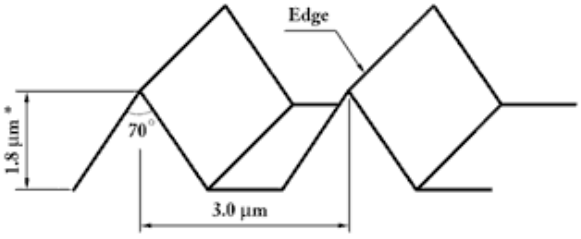

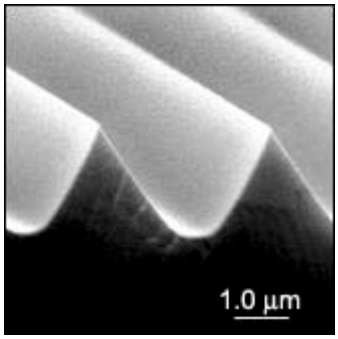

TGG 01, 3 lines of structured area of 1 * 3 mm

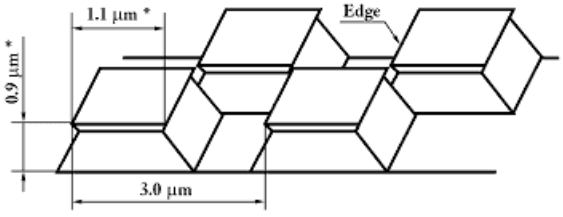

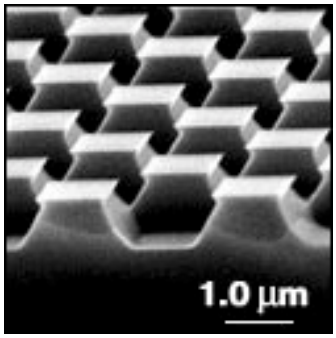

TGX 01, square structured area of 1.5 * 1.5 mm

APPENDIX II

The flat mold design

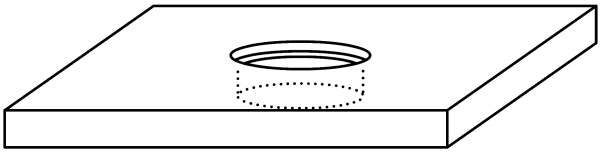

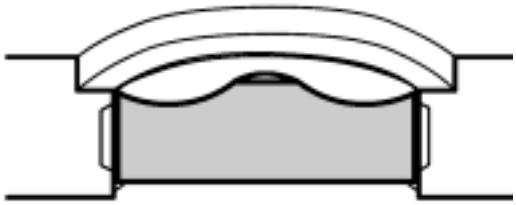

Steel plate with mold

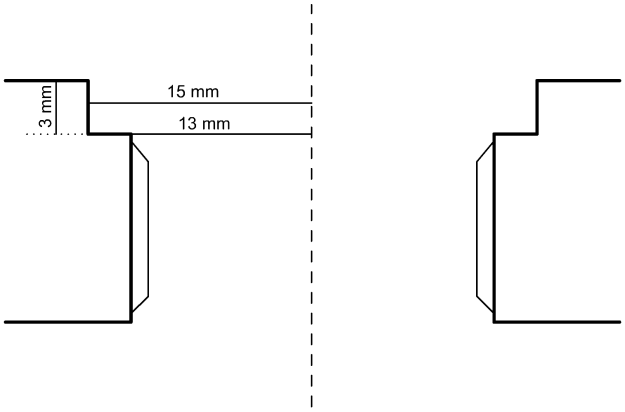

Hole with screw

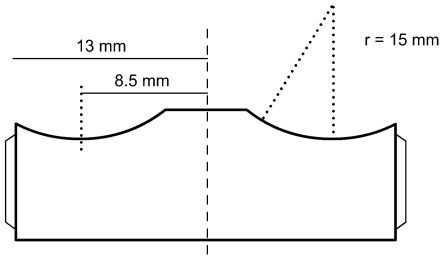

Toroidal inset with screw

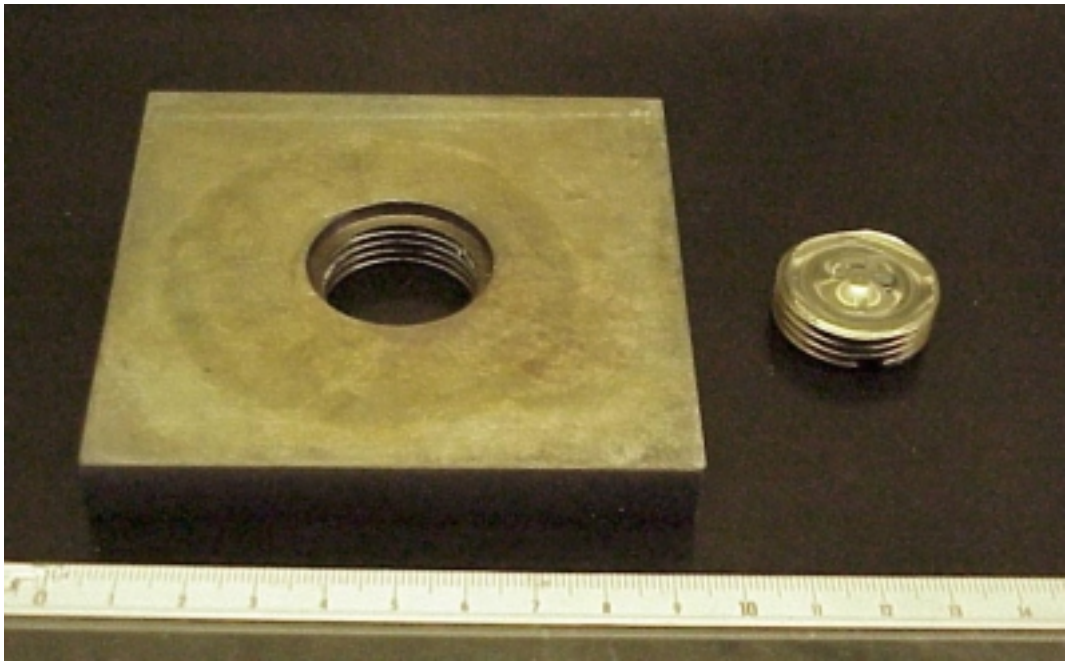

Picture of plate and toroidal inset

Curvature of UHMWPE toroid

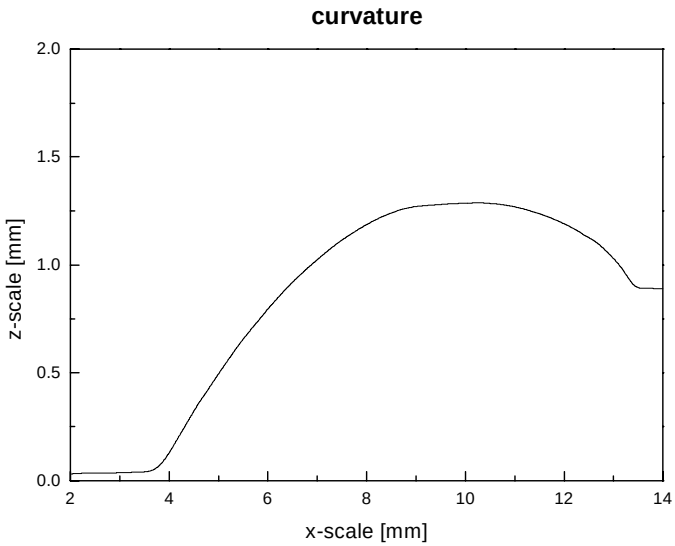

Curvature of UHMWPE toroid, measured linearly from the center outwards in the CETR tribometer

Curvature radius: ~18 mm

APPENDIX III

CETR UMT-2

CETR

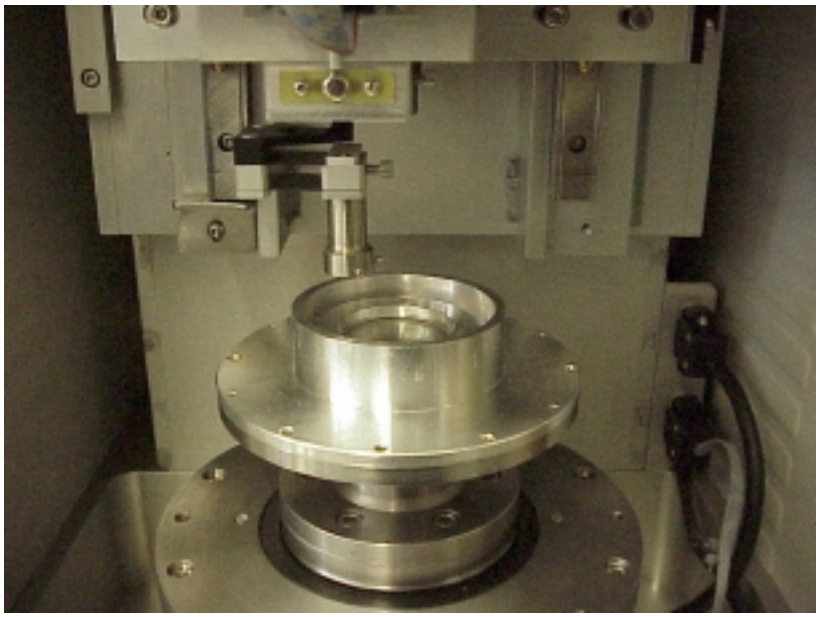

Sample holder for toroid and cylinder

APPENDIX IV

Wear traces on UHMWPE, imaged in optical microscope

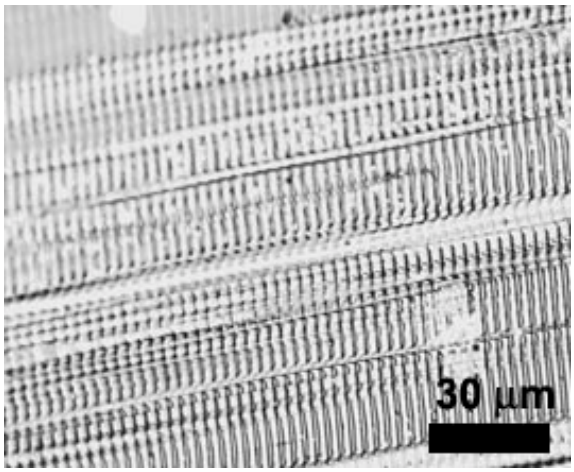

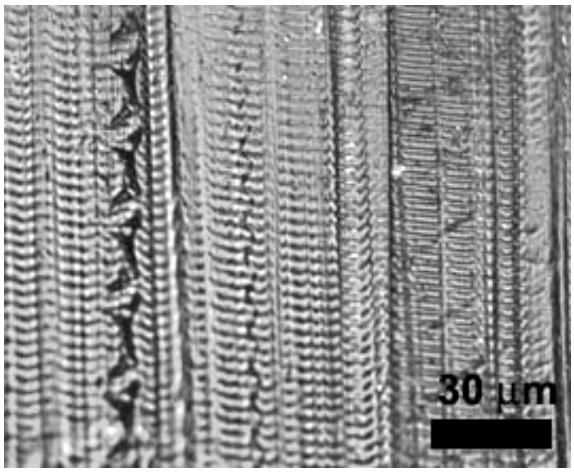

Measured on toroid; scratches through the structure due to ploughing of asperities

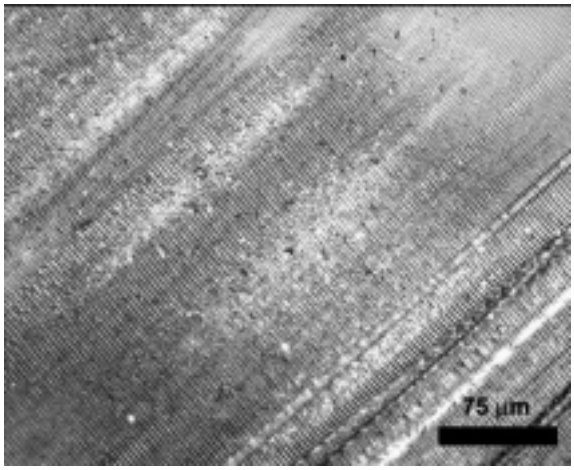

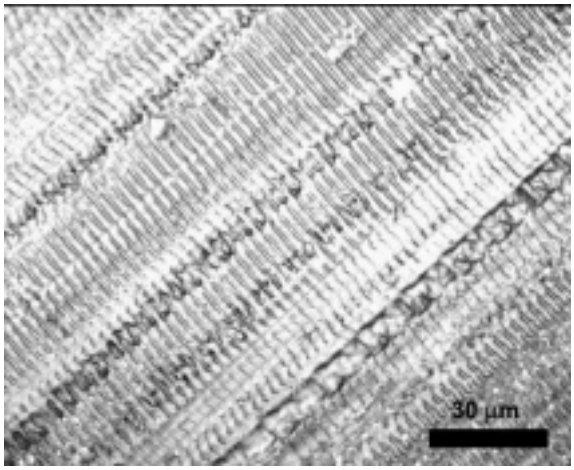

Measured on flat cylinder; fewer big scratches, but still a lot of wear evenly disrtibuted over the contact area

APPENDIX V

Friction of TGG and TGX structured UHMWPE, perpendicular

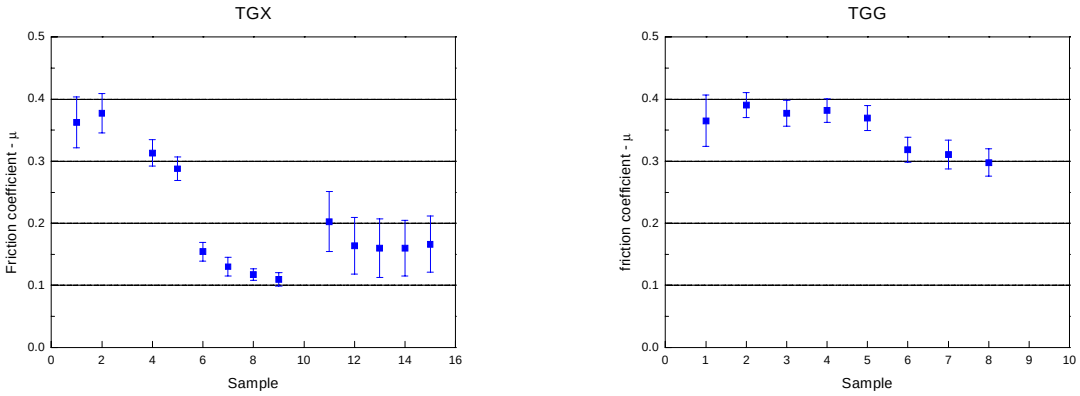

a) b)

Friction coefficient of a) TGX structure; b) TGG structure measured on toroidal geometry on CETR, load 0.1 N, speed 0.1 RPM

Friction measurements at lower loads, UHMWPE, toroidal geometry, lubricated

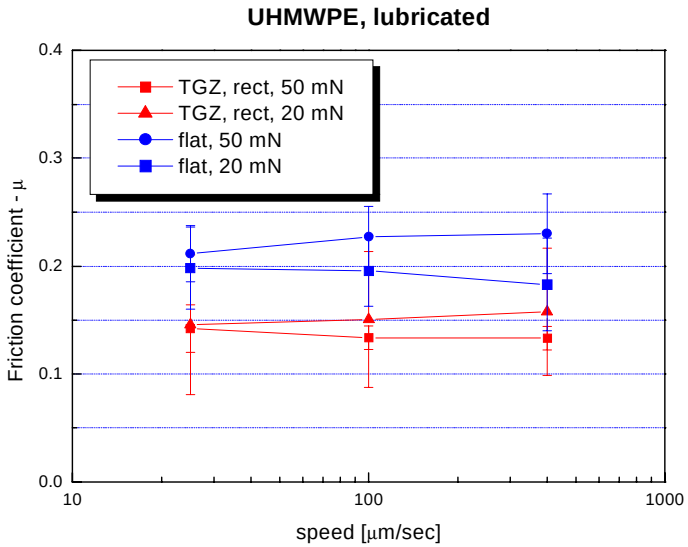

Friction coefficient of UHMWPE under lubricated conditions at different speeds, measured on toroidal geometry; different low loads; flat compared to TGZ03 structure perpendicular to the direction of sliding

Friction traces of linear measurements under lubricating conditions, UHMWPE

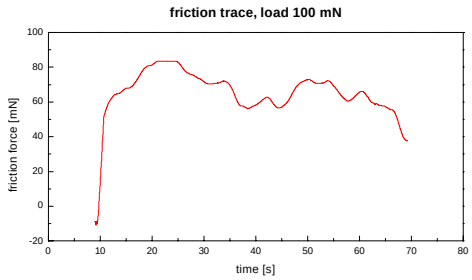

a)

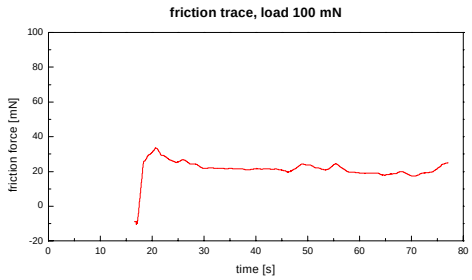

b)

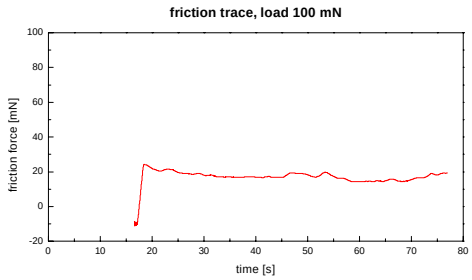

c)

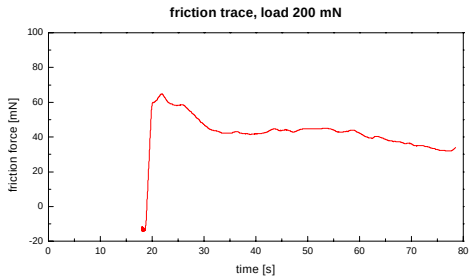

d)

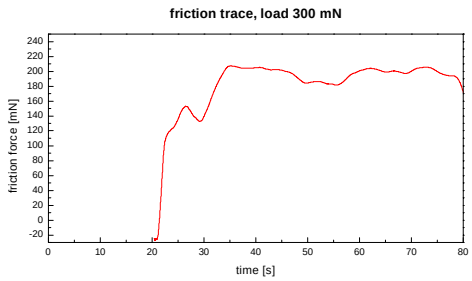

e)

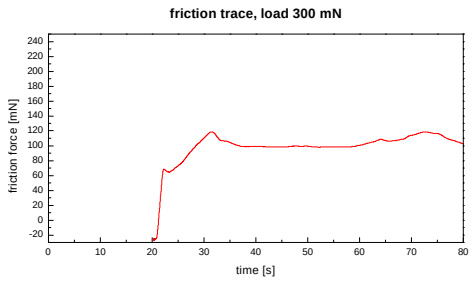

f)

Friction traces measured in order of appearance; these results appear somewhat inconsistent; e and f) on a different friction force scale

APPENDIX VI

AFM images of partially filled grooves achieved by dip coating

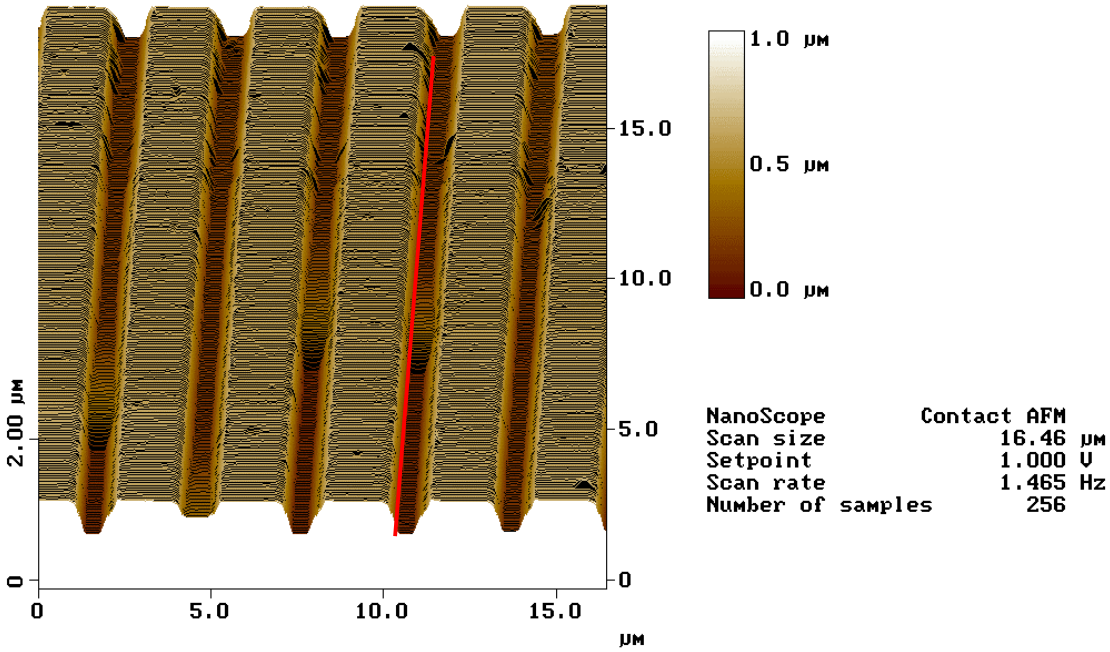

3D image of dip coated structure, taken from the border beyond which the lines are filled with PS; the red line shows the cross section shown below

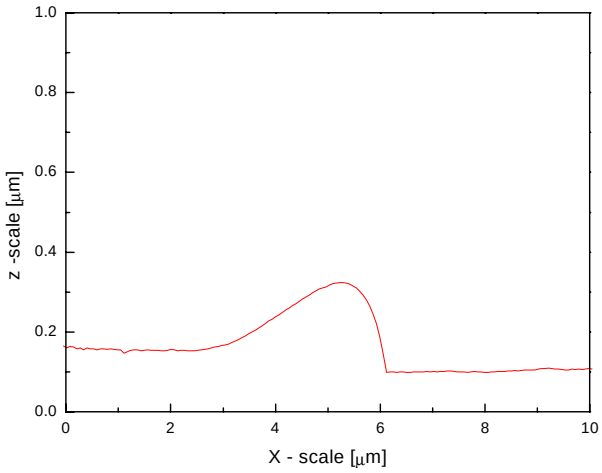

Cross section parallel to the structure, inside a groove, showing the front of a partially filled line